Fe₃O₄-solamargine induces apoptosis and inhibits metastasis of pancreatic cancer cells

XIAODONG XIE[1*], XIUMING ZHANG[1*], JUN CHEN[2], XUN TANG[3],
MEIQIN WANG[1], LEI ZHANG[1], ZHEN GUO[1] and WENRONG SHEN[1]

Departments of [1]Radiology, [2]Intervention and [3]Clinical Laboratory, Jiangsu Cancer Hospital,
Jiangsu Institute of Cancer Research, Nanjing Medical University Affiliated Cancer Hospital,
Nanjing, Jiangsu 210000, P.R. China

Abstract. Fe₃O₄-magnetic liposome (MLP) can deliver drugs to target tissues and can increase drug efficacy. The present study aimed to investigate the effects of solamargine (SM) and Fe₃O₄-SM in pancreatic cancer (PC). Cell viability was detected using a Cell Counting kit-8 assay. Apoptosis and cell cycle progression was tested using a flow cytometry assay. A scratch assay was used to examine cell metastasis. Quantitative polymerase chain reaction, western blot analysis or immunohistochemical analysis were performed to determine the expression of target factors. Magnetic resonance imagining (MRI) and terminal deoxynucleotidyl-transferase-mediated dUTP nick end labelling were conducted to detect tumor growth and apoptosis *in vivo*, respectively. It was demonstrated that Fe₃O₄-SM inhibited cancer cell growth via a slow release of SM over an extended period of time. SM was revealed to induce apoptosis and cell cycle arrest. Furthermore, SM decreased the expression of X-linked inhibitor of apoptosis, Survivin, Ki-67, proliferating cell nuclear antigen and cyclin D1, but increased the activity of caspase-3. It was also observed that SM inhibited tumor cell metastasis by modulating the expression of matrix metalloproteinase (MMP)-2 and TIMP metallopeptidase inhibitor-2. Furthermore, the phosphorylation of protein kinase B and mechanistic target of rapamycin was suppressed by SM. Notably, the effect of SM was enhanced by Fe₃O₄-SM. The malignant growth of PC was decreased by SM *in vivo*. Furthermore, the expression of Ki-67 was decreased by SM and Fe₃O₄-SM. Additionally, cell apoptosis was increased in the Fe₃O₄-SM group, compared with the SM group. The present study illustrated the antitumor effect and action mechanism produced by SM. Additionally, it was demonstrated that Fe₃O₄-SM was more effective than SM in protecting against PC.

Correspondence to: Dr Wenrong Shen, Department of Radiology, Jiangsu Cancer Hospital, Jiangsu Institute of Cancer Research, Nanjing Medical University Affiliated Cancer Hospital, 42 Baiziting, Nanjing, Jiangsu 210000, P.R. China
E-mail: mms_wenrongs@163.com

*Contributed equally

Introduction

Pancreatic cancer (PC) originates in the pancreas and when the pancreatic cells grow uncontrollably, a tumor mass forms. PC cells are able to invade other distant organs within the body (1). The most common type of PC is pancreatic ductal adenocarcinoma, which accounts for ~85% of PC cases (2), and the incidence of PC is increasing. Furthermore, PC is prone to metastasis in the early stages, and such a phenomenon leads to a high mortality rate among patients with PC. In 2015, 411,600 fatalities globally were caused by all types of PC (3). Although the development of surgical techniques and novel drugs is progressing, the 5-year survival rate remains approximately 6% (4). Therefore, investigating novel strategies to treat PC is of clinical significance.

Currently, surgery, radiotherapy and chemotherapy remain the three main traditional tumor therapy methods. However, it is difficult to achieve satisfactory outcomes through applying the traditional treatment methods, as surgery may result in trauma, and radiotherapy and chemotherapy may lead to severe side effects (5). Magnetic targeted drugs delivery system (MTDS), with its high delivery efficiency and good biocompatibility, has attracted much attention since the 1980s (6,7). Magnetic liposome (MLP) was first applied clinically in the 1990s (8,9). Magnetic nanoparticles are composed of a magnetic core and a biocompatible polymeric shell. Under the external magnetic field, the drug-encapsulated magnetic nanoparticles will accumulate in the target tissue area. The drug can then be released from particles in a controlled manner.

The magnetic particles used in nano-magnetic drug carriers are mainly iron monomers, for example, Fe_2O_3, Fe_3O_4 and manganese zinc ferrite complex (10,11). Fe_3O_4 nanoparticles, as one of the ferrites, have been regarded as magnetic nanoparticles in MTDS with good biocompatibility (12,13). The methods for applying an external magnetic field consist of static and alternating magnetic fields (14,15). It has been demonstrated that the drug-loaded magnetic nanoparticles can be gathered by an external magnetic field around the tumor region (16), thereby killing the tumor cells. Magnetic nanoparticles can be applied in magnetic resonance imaging (MRI) visibility and

nanoparticle tracking (17). Therefore, it is of great significance to develop the magnetic targeting drug carrier.

As a steroidal molecule, solamargine (SM) can be isolated from solanum incanum (18). The structure of SM has also been identified previously (19). SM could deliver its effect by simple diffusion via penetrating the cell membrane. SM is belongs to the steroidal molecule family. It has been reported that SM can induce cell death by triggering cell apoptosis in various types of cancer cell (20-22). Nevertheless, the function of SM in PC remains to be investigated. In the present study, the effect of SM and Fe_3O_4-SM was determined, as the effects of a reagent not only rely on the properties itself, but also on the method of reagent delivery. SM was loaded onto Fe_3O_4 MLP to prepare a drug delivery system. The effect of Fe_3O_4-SM on PC was determined by determining cell growth, cell apoptosis and cell cycle progression. The present study also examined the potential mechanism of this. The results of the present study contributed toward the understanding of the effect of SM on PC and provided a novel drug delivery system in treating PC.

Materials and methods

Drugs. Solamargine (SM; CAS No., 20311-51-7; purity, >98%) was purchased from MedChemExpress (Monmouth Junction, NJ, USA).

Preparation of Fe_3O_4 and Fe_3O_4-SM. The chemical precipitation method (23) was adopted to prepare Fe_3O_4. The molar ratio of $Fe^{2+}:Fe^{3+}=1:2$ (a certain amount of $FeSO_4$ and $FeCl_3$) was dissolved in distilled water. Next, 4 mol/ml NaOH (pre-heated to 60°C) was incubated with $FeSO_4$ and $FeCl_3$ mixture with mechanical agitation. The Fe_3O_4 precipitate was then formed. The lecithin/Fe_3O_4 nanoparticle (quality ratio, 10:1) mixture was dissolved in water (the volume of water was equal to 1/5 of the mixture). In brief, the nanoparticles were added into the SM solution and underwent ultrasonic treatment for 6 h. The mixture was then further mixed with ether solution, which contained lecithin and cholesterol. Following rotation for 1 min, the mixture underwent rotary evaporation in a water bath at 37°C. Following emulsion being performed three times, the magnetic nanoparticles were aggregated. Fe_3O_4-SM was separated and purified. A transmission electron microscope (magnification, x120,000) (2000 FX; JEOL, Ltd., Tokyo, Japan) was used to record TEM images. X-ray diffraction (XRD) was performed using Rigaku D/max 2550V (Rigaku Corporation, Tokyo, Japan). Particle size (PCS) analysis was performed using LS13320 (Beckman Coulter, Inc., Brea, CA, USA). The SM content in Fe_3O_4-SM nanocomplex was determined using inductively coupled plasma-mass spectrometry (ICPMS; Optima 5300DV, PerkinElmer, Inc., Waltham, MA, USA).

Cell culture and grouping. The pancreatic cancer BxPC-3 cell line (American Type Culture Collection, Manassas, VA, USA) was cultured in RPMI-1640 medium (Gibco; Thermo Fisher Scientific, Inc., Waltham, MA, USA) supplemented with 10% fetal bovine serum (FBS; Gibco; Thermo Fisher Scientific, Inc.) in a humidified incubator with 5% CO_2 at 37°C. For the subsequent experiments, the cell grouping was as follows: Mock group, tumor cells without any treatment; SM group,

tumor cells were treated with SM for 16 h; and Fe_3O_4-SM group, cells were treated with Fe_3O_4-SM for 16 h. The final concentration of SM in the latter two groups was set at 4.8 μM.

Growth inhibition assay. The cells were seeded into 96-well plates at a density of $1x10^4$ cells/well, prior to being treated with SM or Fe_3O_4-SM for 16 h. The final concentrations of SM were 2.4, 4.8 and 9.6 μM. Cell viability was determined using a CCK-8 assay (Beyotime Institute of Biotechnology, Haimen, China). Absorbance was read on an automated plate reader (Bio-Rad Laboratories, Inc., Hercules, CA, USA) at 450 nm. Cell growth inhibition is presented as the percentage of untreated controls. Growth inhibition was also determined when the cells were treated with SM or Fe_3O_4-SM (final concentration of SM, 4.8 μM) for 12, 18, 24 and 48 h. All determinations were performed in triplicate.

Flow cytometric analysis. Apoptosis was tested using an Annexin V-fluorescein isothiocyanate (FITC)/propidium iodide (PI) kit, according to the manufacturer's protocol. In brief, the tumor cells treated with SM or Fe_3O_4-SM were collected and re-suspended in PBS. Following incubation with Annexin V-FITC for 15 min and with PI for 10 min, cell apoptosis was analyzed using a FACScan flow cytometer (BD Biosciences, Franklin Lakes, NJ, USA). In order to determine cell cycle distribution, the cells were first fixed with 4% paraformaldehyde for 30 min at 4°C, prior to being collected and stained with PI for 30 min at 4°C. FACScan (BD Biosciences) with CELLQuest™ software version 3.3 (BD Biosciences) was used for data analysis.

Determination of caspase-3 activity. At a density of $2x10^6$ cells/well, the cells were incubated with SM or Fe_3O_4-SM at 37°C for 16 h in a 96-well plate. Colorimetric substrate (Ac-DEVD-pNA) was used to detect the activities of caspase-3. The caspase-3 detection kit (cat. no. G007) was purchased from Nanjing Jiancheng Bioengineering Institute (Nanjing, China). The samples were maintained at 37°C and the optical density at 405 nm was measured using an ELISA reader (Multisken Ascent; Thermo Labsystems, Santa Rosa, CA, USA).

Scratch assay. As previously described (24), a scratch assay was performed to detect cell migration. The cells ($1.0x10^6$ cells) were seeded onto the dishes and maintained in an incubator for 8 h. A P200 pipette tip was used to scratch the monolayer. Next, the cells were incubated for another 12 h. The gap distance between the scratch edges was measured by cellSens software (Olympus Corporation, Tokyo, Japan) to determine the cell migration ability.

Cell invasion assay. The invasive ability of the cells was determined using a Transwell assay with Matrigel. In brief, the cells were starved overnight. The cells at a density of $2x10^5$ cells/ml were seeded with Matrigel (BD Biosciences) into the upper chamber of the Transwell. The upper chamber was filled with RPMI-1640 medium without FBS. RPMI-1640 medium containing 15% FBS was plated into the lower chamber of the Transwell. The Transwell was maintained at 37°C for 24 h, allowing the cells to invade into the lower chamber. The invaded cells were harvested and then fixed with 4% paraformaldehyde

Table I. Summary of the reverse transcription-quantitative polymerase chain reaction primers.

Gene	Forward primers (5'-3')	Reverse primers (5'-3')
XIAP	TGTCCCTTTGATTACGGGCT	AAGCCTGTAATCCCAGCACT
Survivin	GTCCCTGGCTCCTCTACTG	GACGCTTCCTATCACTCTATTC
Ki-67	GCCCCTAAAGTAGAACCCGT	GGGTTCGGATGATTTGCCTC
PCNA	CGGATACCTTGGCGCTAGTA	CACTCCGTCTTTTGCACAGG
Cyclin D1	CCCTCGGTGTCCTACTTCAA	CTTAGAGGCCACGAACATGC
MMP-2	ACCACAGCCAACTACGATGA	GCTCCTGAATGCCCTTGATG
MMP-9	GAGACTCTACACCCAGGACG	GAAAGTGAAGGGGAAGACGC
TIMP-2	TGTGTTCCCTCAGTGTGGTT	TTCGGTTTCATTGCGTGTGT
β-actin	CTCCATCCTGGCCTCGCTGT	GCTGTCACCTTCACCGTTCC

XIAP, X-linked inhibitor of apoptosis protein; PCNA, proliferating cell nuclear antigen; MMP, matrix metalloproteinase; TIMP, TIMP metallopeptidase inhibitor.

at 4˚C for 30 min. The cells were then stained with 0.1% crystal violet dye for 20 min at room temperature. The cells were observed under an inverted microscope (magnification, x40).

Quantitative polymerase chain reaction (qPCR). RNAiso Plus (Takara Bio, Inc., Otsu, Japan) was used to isolate total RNA. The RNA was reverse transcribed using M-MLV reverse transcriptase (Promega Corporation, Madison, WI, USA). The synthesized cDNA was subject to subsequent PCR quantification. PCR was performed using SYBR qPCR mix (Toyobo Life Science, Osaka, Japan) on an iCycler (Bio-Rad Laboratories, Inc.). The thermocycling conditions were as follows: 95˚C for 3 min; 33 cycles of 95˚C for 15 sec, 60˚C for 30 sec; a final extension at 72˚C for 10 min. The $2^{-\Delta\Delta Cq}$ method was used for data analysis (25). β-actin mRNA expression was used as a reference. The Primer-BLAST-based sequences are listed in Table I.

Western blot analysis. Cells were lysed in NP40 lysis buffer (Beyotime Institute of Biotechnology) containing protease inhibitors. Following centrifugation at 12,000 x g for 5 min at 4˚C, the protein concentration was detected using a bicinchoninic acid protein quantitative analysis kit (Thermo Fisher Scientific, Inc.). Proteins (20 µg) was separated by 8% SDS-PAGE and transferred onto polyvinylidene difluoride membranes. In order to block non-specific binding, the membranes were incubated with 5% skimmed milk at room temperature for 2 h. The membranes were incubated with primary antibodies against the following: XIAP (cat. no. ab28151; dilution, 1:100), survivin (cat. no. ab208938; dilution, 1:1,000), Ki-67 (cat. no. ab16667, 1:100), PCNA (cat. no. ab29; dilution, 1:200), cyclin D1 (cat. no. ab134175; dilution, 1:10,000), MMP-2 (cat. no. ab92536; dilution, 1:2,000), MMP-9 (cat. no. ab38898; dilution, 1:1,000), TIMP-2 (cat. no. ab1828; dilution, 1:1,000), p-Akt (cat. no. ab131443; dilution, 1:800), Akt (cat. no. ab188099; dilution, 1:2,000), p-mTOR (cat. no. ab109268; dilution, 1:1,000), mTOR (cat. no. ab2732; dilution, 1:2,000) and GAPDH (cat. no. ab8245; dilution, 1:1,000; all Abcam, Cambridge, UK) at 4˚C overnight. The next day, the membranes were incubated with a goat anti-rabbit horseradish peroxidase-conjugated IgG H&L secondary antibody (cat. no. ab6721; dilution, 1:2,000; Abcam). Bands were developed on X-ray film by enhanced chemiluminescence (Beyotime Institute of Biotechnology). The density of the blots was read by using the Quantity One software version 2.4 (Bio-Rad Laboratories, Inc.).

Animals. The Balb/c nude mice (n=25, 4-6 weeks old, 12-15 g, male) were obtained from Shanghai Animal Center. Animals were housed at 22˚C with 40-50% humidity. After being acclimatized, the animals were approved for the experiments. BxPC-3 cells ($1.0x10^7/0.2$ ml) were implanted into the hypoderm of the armpit of the mice to produce pancreatic cancer xenografts. When the diameter reached 3-4 mm, the mice were distributed into the following 4 groups (6 animals/group): Mock group, mice were considered as control; saline group, mice were injected with 0.9% saline by caudal vein injection; SM group, mice were injected with SM by caudal vein injection; Fe_3O_4-SM group, mice were injected with 0.2 ml Fe_3O_4-SM and a round magnet (magnet size was 0.3T; diameter, 25.40 mm; thickness 6.35 mm) was placed externally on the mouse (the magnet was tied using a steel wire under the armpit). The final concentration of SM was 4.8 µM (according to the data from the growth inhibition assay). The largest subcutaneous tumor detected in the present study had a diameter of 1.8 cm and no mice exhibited multiple subcutaneous tumors. According to previous studies (26,27), the humane endpoints were judged by the mouse weight loss (>20% of total body weight) or mouse activity assessment (hunching, stationary, ruffling and poor grooming) and mice were euthanized by O_2/CO_2-asphyxiation and dissected. All the protocols in the animal studies were approved by the Ethics Committee of Jiangsu Cancer Hospital (Nanjing, Jiangsu, China).

Tumor volume assessment and MRI imaging. The nude mice bearing xenografts were injected with saline (0.9%), SM or Fe_3O_4-SM by caudal vein injection. On the seventh, fourteenth and twenty first days after the injection, MRI scans were performed on the mice. MRI was conducted using a 1.5 Tesla scanner (INTERA ACHIEVA 1.5T; Philips Medical Systems) with SENSE-body coil. The tumor exhibited a high-signal intensity on T2-weighted images. The longitudinal diameter (d1) on the sagittal images, the anteroposterior diameter (d2) on the sagittal images and the largest lateral diameter (d3) on the axial images were measured. The diameter-based calculations for tumor volume were calculated as d1 x d2 x d3 x π/6.
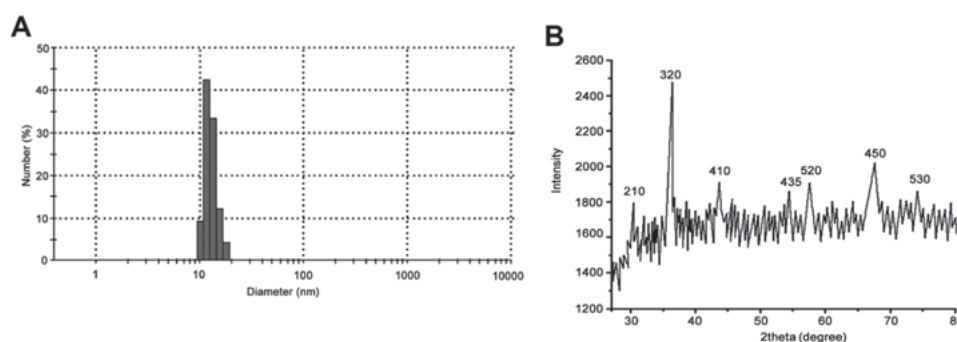
Figure 1. Identification of Fe$_3$O$_4$-MLP. (A) Particle size distribution of Fe$_3$O$_4$-MLP measured by particle size. (B) X-ray diffraction imaging of Fe$_3$O$_4$-MLP. MLP, magnetic liposome.
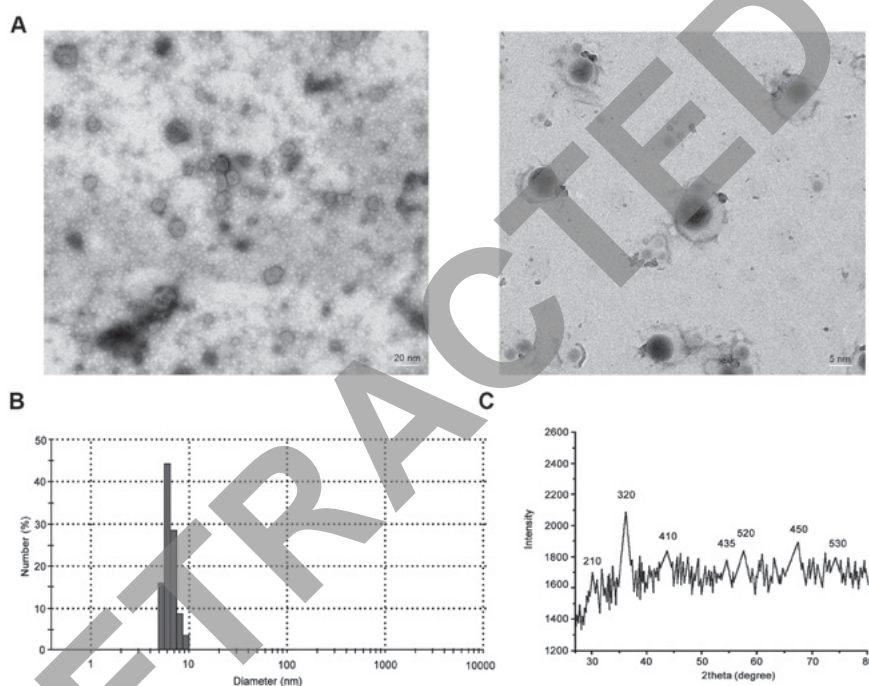

Figure 2. Imaging and size distribution of Fe$_3$O$_4$-SM. (A) Transmission electron microscopy images for Fe$_3$O$_4$-SM. (B) The particle size distribution of Fe$_3$O$_4$-SM measured by particle size. (C) X-ray diffraction imaging of Fe$_3$O$_4$-SM. SM, solamargine.

H&E staining and immunohistochemistry (IHC). The animals were sacrificed and the tumor mass were excised. Following fixing with 4% paraformaldehyde overnight at 4˚C, the samples were dehydrated in a graded ethanol series, followed by routine paraffin embedding and sectioning (3-4 μm). The paraffin-embedded tissue sections were subjected to H&E staining and IHC. The sections were subjected to deparaffinization by washing with xylene and rehydration in a graded ethanol series. Slides were boiled by immersing them in a sodium citrate buffer (pH 6.0, 10 mM) and heated to 95˚C for antigen retrieval. The cooled sections were then incubated in 3% hydrogen peroxide for 10 min at room temperature. Following incubation with 10% normal goat serum (Beyotime Institute of Biotechnology) for 30 min at 37˚C, the sections were maintained with primary anti-Ki-67 antibody (cat. no. ab15580; dilution, 1:100, Abcam) at 4˚C overnight. Biotin-labeled secondary antibodies were the incubated with the sections at room temperature for 1 h, prior to incubation with horseradish peroxidase-conjugated streptavidin for 30 min at room temperature. Slides were

stained with diaminobenzidine (DAB) for 5 min at room temperature. Next, Mayer's hematoxylin (Sangon Biotech Co., Ltd., Shanghai, China) was incubated with the slides for 2 min at room temperature. The sections were observed using a light microscope (magnification, x100). Finally, the sections were mounted with neutral balsam (Beijing Solarbio Science & Technology Co., Ltd., Beijing, China).

Terminal deoxynucleotidyl transferase dUTP nick end labelling (TUNEL) staining. TUNEL was conducted using TUNEL assay kit (Roche Diagnostics, Basel, Switzerland), according to the manufacturer's protocol. In brief, the tissues were fixed with 4% paraformaldehyde overnight at 4˚C. Xylene was used for deparaffinization of the paraffin-embedded sections. Terminal deoxynucleotidyl transferase (TdT) enzyme was incubated with sections for 1 h at 37˚C. The sections were incubated with 0.3% H$_2$O$_2$ for 3 min at room temperature. The nuclei were stained with 50 μl DAB working solution for 10 min at room temperature. The slides were counterstained with hematoxylin and mounted
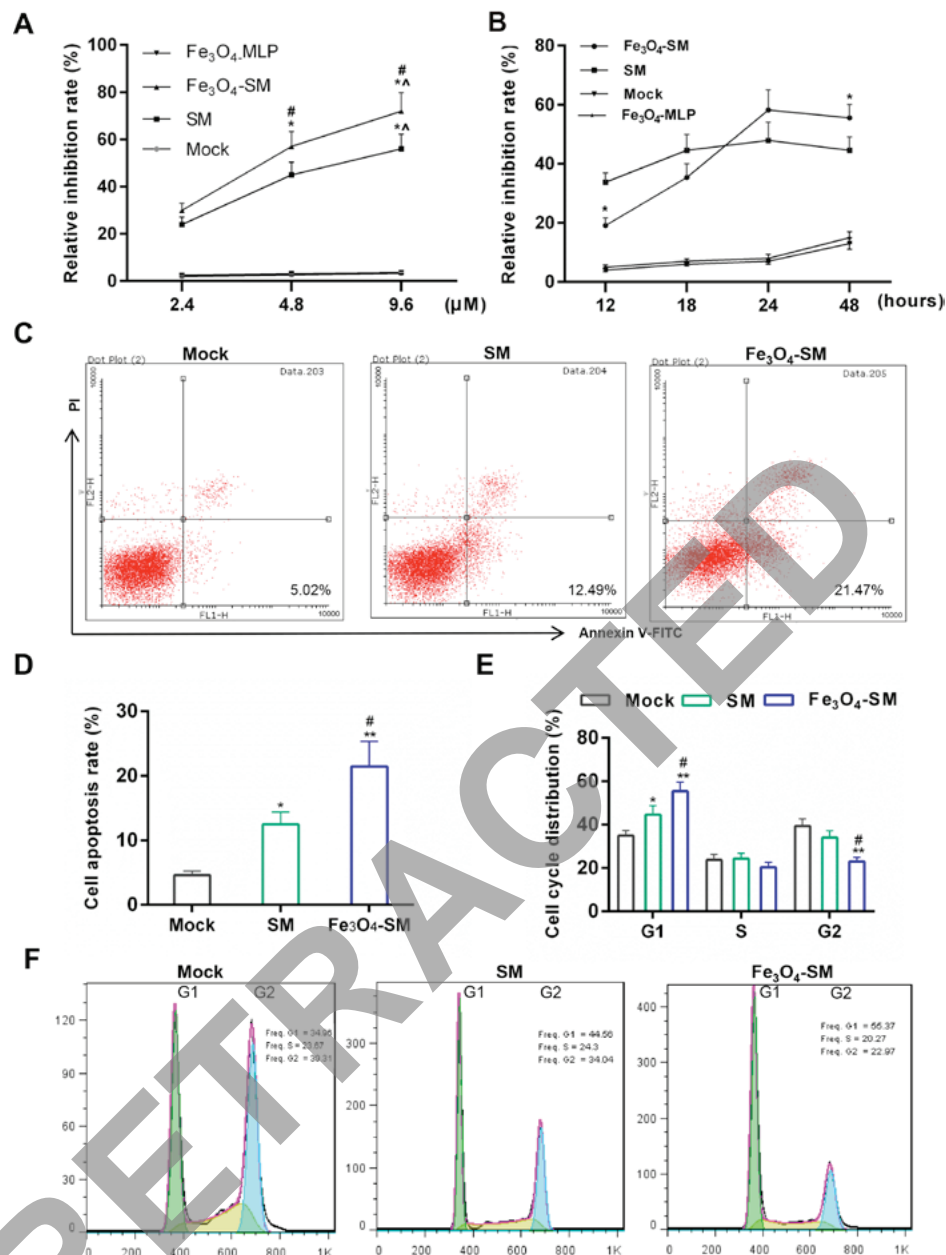
Figure 3. Effects of Fe_3O_4-SM on the cell apoptosis and cell cycle. (A) Effect of SM on growth inhibition at different concentrations was detected by Cell Counting kit-8 assay. The PC cells were treated with SM, Fe_3O_4-SM or Fe_3O_4-magnetic liposome for 16 h, the untreated PC cells acted as control. *P<0.05 vs. 2.4 μM; ^P<0.05 vs. 4.8 μM; #P<0.05 vs. SM group. (B) Growth inhibition at different time-points. The PC cells were treated with SM or Fe_3O_4-SM, and viability was detected after 12, 18, 24 and 48 h. *P<0.05 vs. SM group. (C and D) Apoptosis detection by FCM; (E and F) Cell cycle distribution determined by FCM. Mock, PC cells without treatment; SM, cells treated with SM; Fe_3O_4-SM, cells treated with Fe_3O_4-SM; *P<0.05, **P<0.01 vs. Mock group; #P<0.05 vs. SM group. SM, solamargine; PC, pancreatic cancer; FCM, flow cytometry.

with neutral balsam. A light microscope was used to observe the cell staining (magnification, x100). The percentage of apoptotic cells was determined by counting TUNEL-positive cells. The brown staining demonstrated apoptotic cells and the blue staining demonstrated non-apoptotic cells. Five randomly selected fields was observed.

Statistical analysis. P<0.05 was considered to indicate a statistically significant difference. Prism Graphpad version 6.0 software (GraphPad Software, Inc., La Jola, CA, USA) was used to analyze the data. Data was shown as mean ± standard deviation. One-way analysis of variance followed by Tukey's multiple comparisons test.

Results

Identification of Fe_3O_4-MLP. As demonstrated in Fig. 1A, the average particle size of Fe_3O_4-MLP was 11.9 nm. The results from XRD demonstrated that the diffraction peaks of Fe_3O_4-MLP were 210, 320, 410, 435, 520, 450 and 533. The results were in line with the characteristic peak of Fe_3O_4 nanoparticles (Fig. 1B). The average particle size of Fe_3O_4-SM was 5-6 nm (Fig. 2A and B). The diffraction peaks of Fe_3O_4-SM were similar to that of Fe_3O_4-MLP (Fig. 2C).

Effect of Fe_3O_4-SM on cell viability in vitro. As demonstrated in Fig. 3A, the Fe_3O_4-MLP treatment did not decrease cell
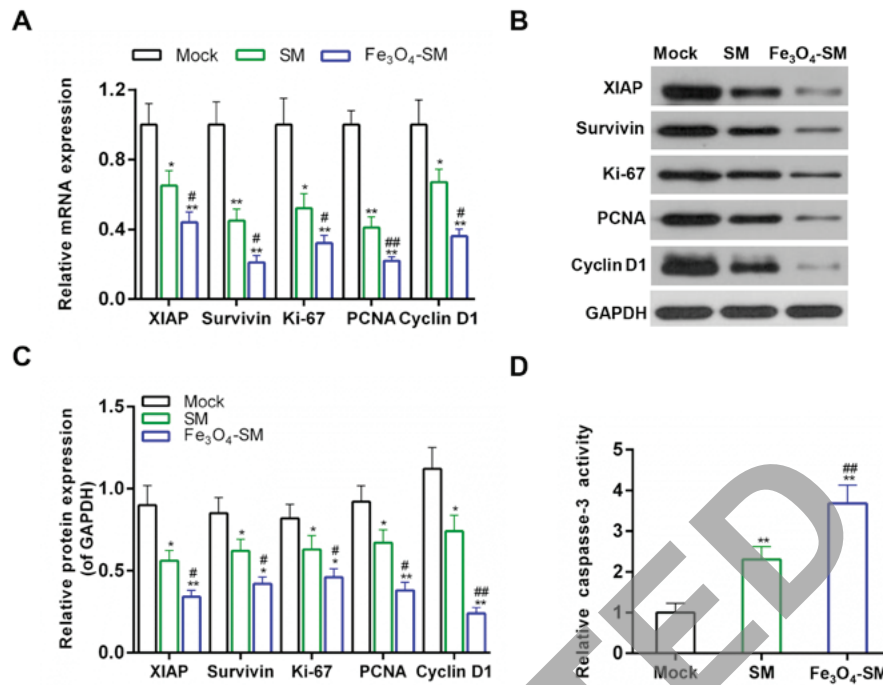
Figure 4. Effects of Fe$_3$O$_4$-SM on the expression of cell apoptosis-related and cell cycle-related genes. (A) Quantitative polymerase chain reaction for the mRNA expression of XIAP, Survivin, Ki-67, PCNA and cyclin D1; (B and C) western blot analysis for the protein expression of XIAP, survivin, Ki-67, PCNA and cyclin D1; and (D) the caspase-3 activity measured by ELISA; *P<0.05, **P<0.01 vs. Mock group; #P<0.05, ##P<0.01 vs. SM group. SM, solamargine; XIAP, X-linked inhibitor of apoptosis; PCNA, proliferating cell nuclear antigen.

growth. Compared with the Mock group, the cell viability was first depressed by SM (P<0.05) and was then further inhibited by Fe$_3$O$_4$-SM (P<0.05). The effect of SM occurred in a dose-dependent manner. Furthermore, CCK-8 results demonstrated that during 12-18 h, the cell growth inhibition effect produced by SM was stronger than that generated by Fe$_3$O$_4$-SM. However, the inhibitory effect of Fe$_3$O$_4$-SM was greater than that of SM after 24 h (Fig. 3B; P<0.05). The results demonstrated that the Fe$_3$O$_4$-SM exerted its antitumor effect slowly.

Effect of Fe$_3$O$_4$-SM on apoptosis and cell cycle progression in vitro. Subsequently, apoptosis and cell cycle progression were determined. Flow cytometric results demonstrated that apoptosis was first induced by SM (P<0.05) and then further enhanced by Fe$_3$O$_4$-SM (P<0.05; Fig. 3C and D). Furthermore, compared with the mock group, the cell numbers in the G1 phase during the cell cycle progression were higher in the SM (P<0.05) and Fe$_3$O$_4$-SM (P<0.01) groups. However, the cell percentage in G2 phase was reduced in the SM and Fe$_3$O$_4$-SM groups (P<0.05). Fe$_3$O$_4$-SM was revealed to significantly enhance the effect of SM (Fig. 3E and F; P<0.05). To further confirm the pro-apoptotic effect of Fe$_3$O$_4$-SM, the expression of proliferation-related and apoptosis-related molecules was determined. The results demonstrated that the expression of XIAP, survivin, Ki-67, PCNA and cyclin D1 were decreased at the transcriptional and translational levels in the SM and Fe$_3$O$_4$-SM groups. Treatment with Fe$_3$O$_4$-SM further increased the effect of SM (P<0.05; Fig. 4A-C). The activity of caspase-3 was also tested, and data from ELISA revealed that the active caspase-3 activity was also increased in the Fe$_3$O$_4$-SM group, compared with the SM group (P<0.01; Fig. 4D).

Effect of Fe$_3$O$_4$-SM on tumor cell migration and invasion in vitro. Metastasis is also a common and typical phenotype of cancer. Therefore, the effect of Fe$_3$O$_4$-SM on cell migration and invasion ability was examined. Fig. 5A demonstrated that the wound thickness was larger in the SM and Fe$_3$O$_4$-SM (P<0.01) groups, suggesting that the cell migration ability was depressed. Furthermore, it was demonstrated that the cell migration ability was dampened more by Fe$_3$O$_4$-SM than by SM. Additionally, cell invasion was further inhibited by Fe$_3$O$_4$-SM, compared with the SM group (P<0.01; Fig. 5B). The expression of molecules associated with tumor metastasis was also detected. The results of the present study demonstrated that the expression of MMP-2 was decreased more in the Fe$_3$O$_4$-SM group than in SM group (P<0.05). However, the expression of MMP-9 exhibited no significant changes among these groups. By contrast, the expression of TIMP-2 was higher in the Fe$_3$O$_4$-SM group than that in the SM group (P<0.05; Fig. 5C-E).

Effect of Fe$_3$O$_4$-SM on the Akt/mTOR signaling pathway. To illustrate the underlying mechanisms, the activity of the Akt/mTOR signaling pathway was determined. The results revealed that the expression of p-Akt and p-mTOR was decreased by SM (P<0.05), compared with the Mock group. Furthermore, treatment with Fe$_3$O$_4$-SM further enhanced the effect of SM (P<0.01; Fig. 6A and B).

Fe$_3$O$_4$-SM inhibits tumor growth and induces tumor apoptosis in vivo. The effect produced by Fe$_3$O$_4$-SM was estimated in vivo. MRI was employed to assess tumor size and volume. MRI images revealed that the tumor volume increased as time progressed. However, the tumor growth rates in the SM
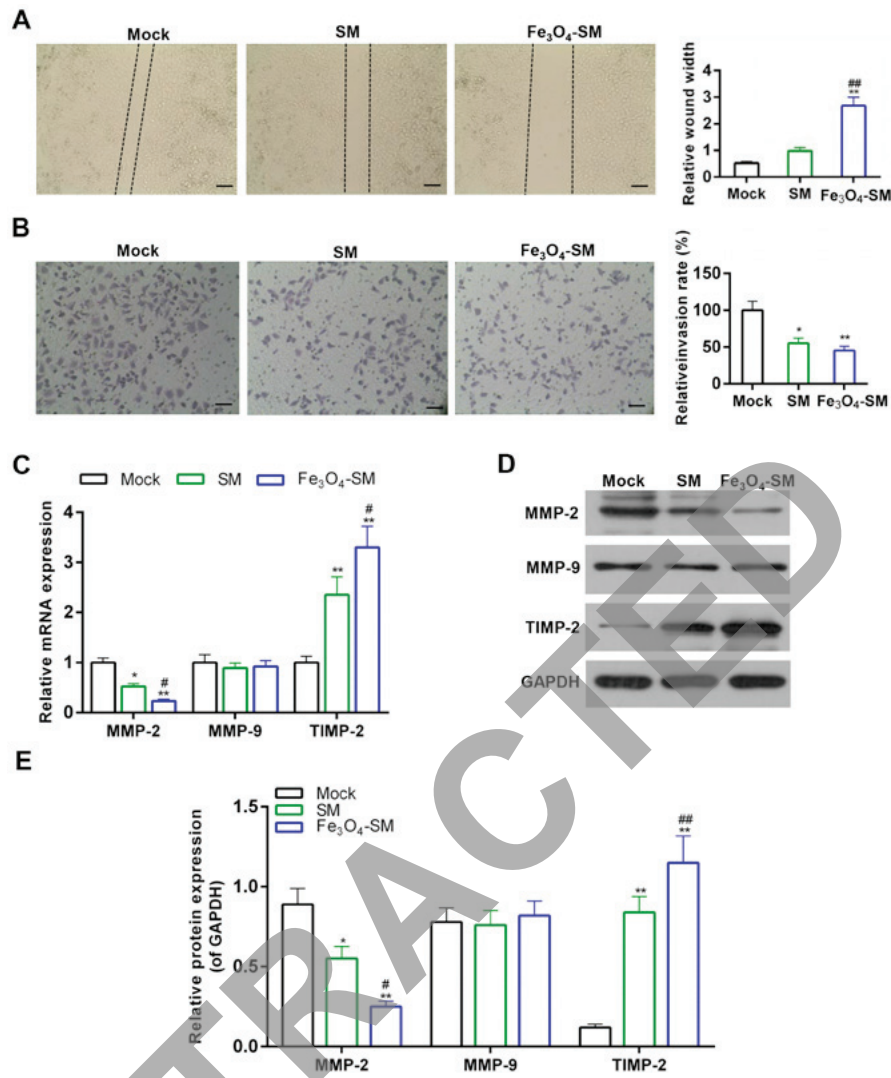
Figure 5. Effects of Fe$_3$O$_4$-SM on cell invasion and migration. (A) Scratch assay for cell migration; scale bar, 20 μm. (B) Transwell assay for cell invasion.; scale bar, 20 μm. (C) Quantitative polymerase chain reaction for the mRNA expression of MMP-2, MMP-9 and TIMP-2. (D and E) Western blot analysis for the protein expression of MMP-2, MMP-9 and TIMP-2. *P<0.05, **P<0.01 vs. Mock group; #P<0.05, ##P<0.01 vs. SM group. SM, solamargine; MMP, matrix metalloproteinase; TIMP, TIMP metallopeptidase inhibitor.
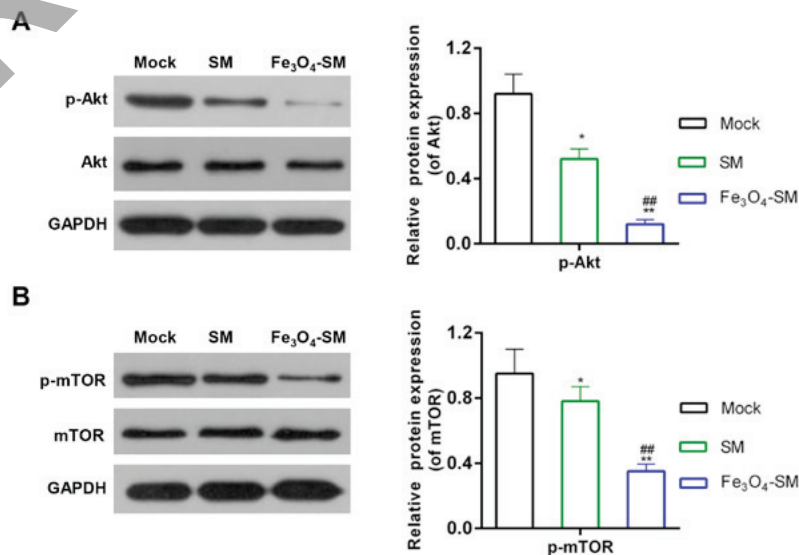

Figure 6. Effects of Fe$_3$O$_4$-SM on the activity of the Akt/mTOR signaling pathway. Western blot analysis for the protein expression of (A) p-Akt and (B) p-mTOR. *P<0.05, **P<0.01 vs. Mock group; ##P<0.01 vs. SM group. SM, solamargine; p-Akt, phosphorylated protein kinase B; p-mTOR, phosphorylated mechanistic target of rapamycin.
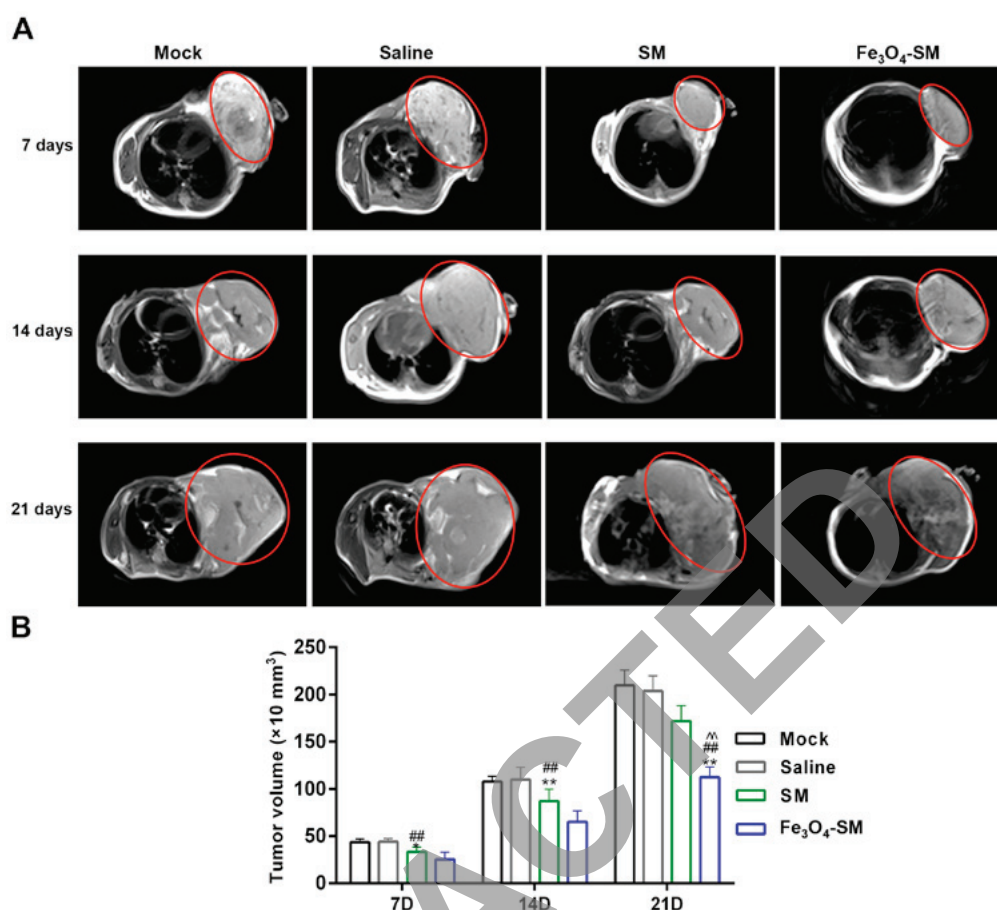
Figure 7. Effect of Fe_3O_4-SM on tumor volume. (A) Tumor volume was measured by magnetic resonance imaging. (B) The determination of tumor volume. [*]P<0.05, [**]P<0.01 vs. Mock group; [##]P<0.01 vs. saline group; [^^]P<0.01 vs. SM group.

and Fe_3O_4-SM groups were slower than those in the mock and saline groups. After 21 days, the tumor volume, size and weight in the Fe_3O_4-SM group was the smallest and lightest among these four groups (P<0.01; Figs. 7A and B and 8A). Furthermore, H&E staining demonstrated that, compared with the SM group (Fig. 8B), the tumor malignance was first decreased by SM (P<0.05), and then further inhibited by Fe_3O_4-SM (P<0.05). To further confirm the antitumor effect of Fe_3O_4-SM, the expression of Ki-67 was determined by IHC. The assay demonstrated that the expression of Ki-67 was suppressed by SM and Fe_3O_4-SM (P<0.01; Fig. 9A). In addition, the TUNEL assay demonstrated that SM significantly induced apoptosis, and Fe_3O_4-SM further enhanced the apoptosis mediated by SM (P<0.01; Fig. 9B).

Discussion

Although surgery, and/or radiotherapy and chemotherapy have been the standard methods used to treat PC (28), drug-loaded MLP has also attracted a great deal of attention (29). Furthermore, traditional Chinese medicines have been recognized as having a strong capability of modulating cell activities (30). SM, a main active component from solanum incanum, exerts antitumor effects in multiple tumor types (21,31,32). Therefore, the present study investigated the effect of SM on PC. It was revealed that SM inhibited tumor cell growth in a dose-dependent manner. Drug-loaded

MLP delivered the agent directly to the targeted tissues and released the drug in a controlled manner, thereby reducing the drug dosage required and the number of toxic side effects. Therefore, Fe_3O_4-SM was prepared to aid in determining the effect produced by Fe_3O_4-SM on PC. It was demonstrated that Fe_3O_4-MLP alone did not inhibit tumor cell growth. However, although Fe_3O_4-SM increased the drug effectiveness of SM, it decreased the release rate of SM. This suggested that the growth inhibition effect of Fe_3O_4-SM was mediated by SM.

The 'suicidal' behavior of cells is mainly regulated by apoptosis, which is a research focus of oncology. Induction of apoptosis is considered as an action mechanism of the majority of antitumor regents (33). Therefore, cell apoptosis was examined following the cells were being treated with SM or Fe_3O_4-SM. FCM data demonstrated that SM caused tumor cell death by apoptosis, which was enhanced by Fe_3O_4-SM. Furthermore, disorder of cell cycle progression may cause tumor formation (34). As the number of dividing cells is larger in tumors than in normal tissues, it leads to the malignant proliferation of tumor cells. The cells in active division may be the targets of drugs in tumor therapy. The results of the present study revealed that SM induced G1 cell cycle arrest. Similarly, the Fe_3O_4-SM enhanced the effect of SM. Furthermore, numerous molecules, including XIAP (35), Survivin (36), Ki-67 (37), PCNA (38) and cyclin D1 (39), participate in tumor cell growth, apoptosis and cell cycle progression. The results of the present study revealed that the expression of
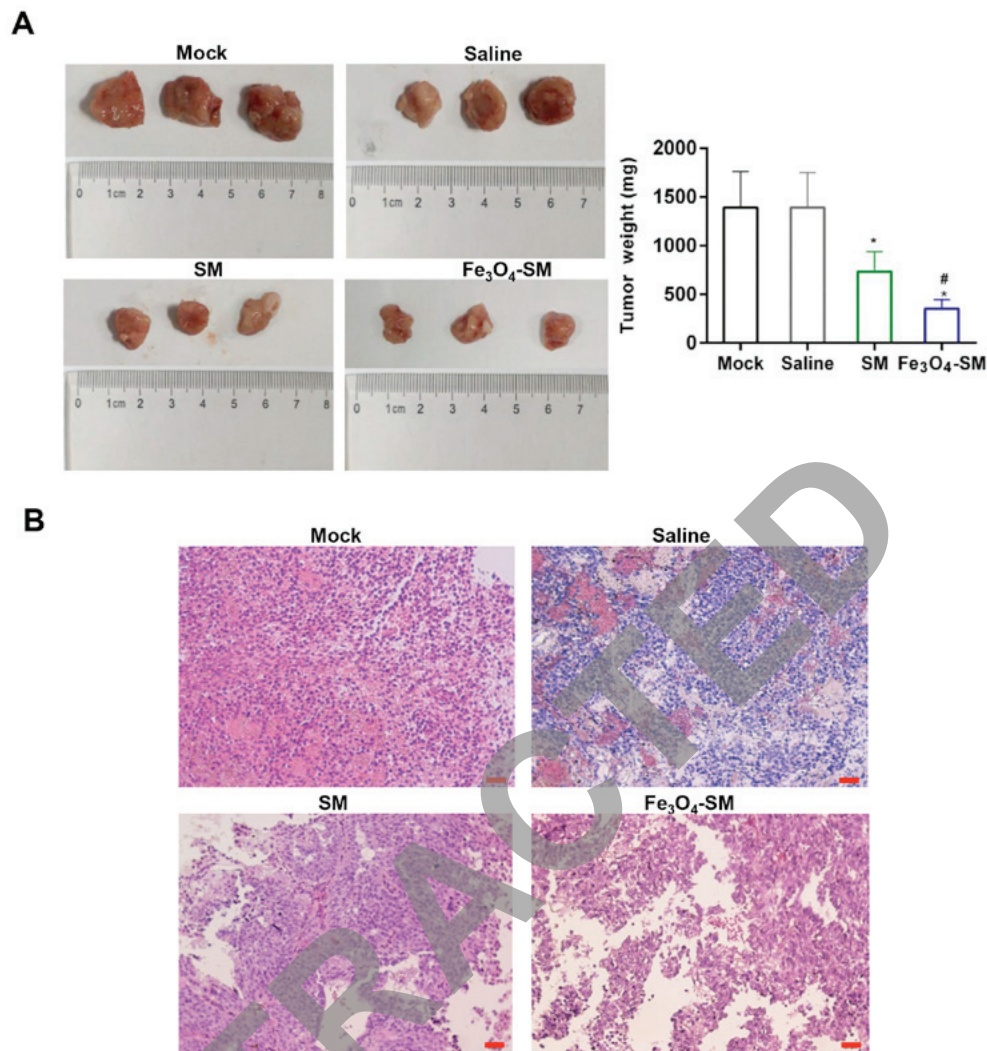
Figure 8. Effect of Fe_3O_4-SM on tumor growth. (A) Preventative images for diameter of PC xenografts and the tumor weight of PC xenografts; (B) H&E staining for the malignant growth of xenografts tissues. Scale bar, 20 μm. PC, pancreatic cancer. *P<0.05 vs. saline group; #P<0.05 vs. SM group.
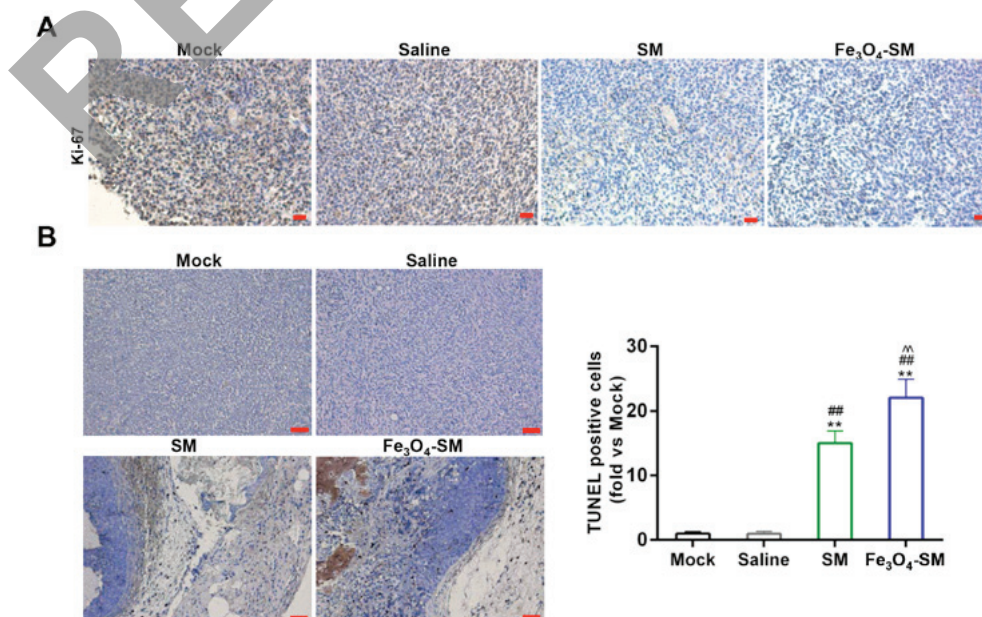

Figure 9. Effect of Fe_3O_4-SM on tumor apoptosis. (A) Immunohistochemical staining for the expression of Ki-67. (B) Terminal deoxynucleotidyl transferase dUTP nick end labelling staining was performed to detect the apoptosis of xenografts tissues. **P<0.01 vs. Mock group; ##P<0.01 vs. Saline group; ^^P<0.01 vs. SM group. Scale bar, 20 μm.

these genes was regulated by SM and Fe_3O_4-SM. Activation of caspase-3 was the convergence of several apoptotic pathways. The activity of caspase-3 was higher in Fe_3O_4-SM-treated cells than in SM-treated cells, and this phenomenon confirmed the antitumor effect of SM. Taken together, the results of the present study demonstrated that SM exerted its antitumor effect by inducing apoptosis and cell cycle arrest, and that the effect of SM was enhanced by Fe_3O_4-SM.

Distant metastasis is a common characteristic of malignant tumors and is a major cause of refractory tumors (40). Data from scratch assay and Transwell assay demonstrated that cell migration and invasion were further depressed by Fe_3O_4-SM, compared with SM, indicating that Fe_3O_4-SM may have the potential to block metastasis in clinical practice. MMP-2 and MMP-9, which are two MMP family members, are associated with the metastatic potential of tumors. TIMP-2 is an inhibitor of MMP-2 (41), and the balance between MMPs and TIMP is crucial to tumor metastasis. The results of the present study demonstrated that the expression of MMP-2 was decreased by SM; the expression of TIMP-2 was increased by SM, The effect of SM was enhanced following loaded on Fe_3O_4. The expression of MMP-9 remained relatively stable in the present study. Previous studies have reported that high expression of MMP-2 contributed toward the promotion of tumor metastasis (42,43), suggesting that SM may mediate its antitumor effect by inhibiting tumor metastasis.

The association between Akt-mTOR tango and cancer has been previously reported (44). To illustrate the molecular mechanism of SM, the activity of the Akt/mTOR signaling pathway was determined in the present study. The results of the present study demonstrated that the expression of p-Akt and p-mTOR was decreased by the effect produced by SM. The efficacy of SM was increased by the encapsulation of Fe_3O_4-MLP. Consistently, Akt and mTOR phosphorylation have been identified in multiple tumor types (45-47). Therefore, the Akt/mTOR pathway may be considered as a target of cancer therapy (48).

Finally, the present study investigated the effect delivered by SM *in vivo*. MRI is a powerful non-invasive and in situ real time detection method for the diagnosis of cancer (49). The MRI image demonstrated that the tumor volume was decreased by the effect mediated by SM, compared with the mock and saline groups. The present study also demonstrated that Fe_3O_4-MLP was an effective MRI contrast agent. The data of tumor diameter was consistent with the MRI results. Furthermore, the malignant proliferation was inhibited by Fe_3O_4-SM more than by SM. Furthermore, Fe_3O_4-SM further depressed the staining for Ki-67, compared with SM. The proportion of apoptotic cells was increased in the Fe_3O_4-SM group, compared with the SM group. Therefore, these data confirmed the antitumor effect mediated by SM *in vivo*.

To the best of our knowledge, the present study was the first to demonstrate the protective effect of SM on pancreatic cancer (PC). The present study demonstrated that Fe_3O_4-SM enhanced the antitumor effect of SM. The action mechanism of SM was determined by inducing apoptosis and cell cycle arrest, and by suppressing tumor cell metastasis. Inhibition of the Akt/mTOR signal pathway was observed to promote the antitumor effect mediated by SM. In conclusion, the *in vitro* and *in vivo* results of the present study proved that SM produced an antitumor effect, and that Fe_3O_4-MLP may be an

effective delivery agent in PC treatment. Therefore, the present study provided an alternative strategy for PC therapy.

Availability of data and materials

The analyzed datasets generated during the present study are available from the corresponding author on reasonable request.

Authors' contributions

XX wrote the main manuscript. XX, XZ, JC, XT, MW, LZ and ZG performed the experiments. XX, XZ, JC and WS designed the study. XC, XZ, JC, XT, MW, LZ and WS performed data analysis. XC, XZ, JC and WS contributed to manuscript revisions. All authors reviewed the manuscript. All authors read and approved the final manuscript.

Ethics approval and consent to participate

All the protocols in the animal studies were approved by the Ethics Committee of Jiangsu Cancer Hospital (Nanjing, Jiangsu, China).

Patient consent for publication

Not applicable.

Competing interests

The authors declare that they have no competing interests.

References

1. Raimondi S, Lowenfels AB, Morselli-Labate AM, Maisonneuve P and Pezzilli R: Pancreatic cancer in chronic pancreatitis; aetiology, incidence, and early detection. Best Pract Res Clin Gastroenterol 24: 349-358, 2010.
2. No authors listed: The World Cancer Report - the major findings. Cent Eur J Public Health 11: 177-179, 2003.
3. GBD 2016 Causes of Death Collaborators: Global, regional, and national age-sex specific mortality for 264 causes of death, 1980-2016: A systematic analysis for the Global Burden of Disease Study 2016. Lancet 390: 1151-1210, 2017.
4. Kleeff J, Michalski C, Friess H and Büchler MW: Pancreatic cancer: From bench to 5-year survival. Pancreas 33: 111-118, 2006.
5. Schiff E and Ben-Arye E: Complementary therapies for side effects of chemotherapy and radiotherapy in the upper gastrointestinal system. Eur J Integr Med 3: 11-16, 2011.
6. Gupta AK and Gupta M: Synthesis and surface engineering of iron oxide nanoparticles for biomedical applications. Biomaterials 26: 3995-4021, 2005.
7. Gan ZJJ: Preparation of magnetic monodisperse nanoparticles and biopolymer assembly on the magnetic carriers. Huaxue Jinzhan 17: 978-986, 2005.

8. Gallo JM and Hafeli U: A.S. Lübbe *et al.*, Preclinical experiences with magnetic drug targeting: tolerance and efficacy. Cancer Res, 56: 4694-4701, 1996; and Clinical experiences with magnetic drug targeting: a phase I study with 4'-epidoxorubicin in 14 patients with advanced solid tumors. Cancer Res 56: 4686-4693, 1996. Cancer Res 57: 3063-3065, 1997.
9. Lübbe AS, Bergemann C, Riess H, Schriever F, Reichardt P, Possinger K, Matthias M, Dörken B, Herrmann F, Gürtler R, *et al*: Clinical experiences with magnetic drug targeting: A phase I study with 4'-epidoxorubicin in 14 patients with advanced solid tumors. Cancer Res 56: 4686-4693, 1996.
10. Sabaté R, Barnadas-Rodríguez R, Callejas-Fernández J, Hidalgo-Alvarez R and Estelrich J: Preparation and characterization of extruded magnetoliposomes. Int J Pharm 347: 156-162, 2008.
11. Fricker J: Drugs with a magnetic attraction to tumours. Drug Discov Today 6: 387-389, 2001.
12. Kohler N, Sun C, Wang J and Zhang M: Methotrexate-modified superparamagnetic nanoparticles and their intracellular uptake into human cancer cells. Langmuir 21: 8858-8864, 2005.
13. Cinteza LO, Ohulchanskyy TY, Sahoo Y, Bergey EJ, Pandey RK and Prasad PN: Diacyllipid micelle-based nanocarrier for magnetically guided delivery of drugs in photodynamic therapy. Mol Pharm 3: 415-423, 2006.
14. Novikov VV, Ponomarev VO, Novikov GV, Kuvichkin VV, Iablokova EV and Fesenko EE. Effects and molecular mechanisms of the biological action of weak and extremely weak magnetic fields. Biofizika 55: 565-572, 2010.
15. Sato K, Watanabe Y, Horiuchi A, Yukumi S, Doi T, Yoshida M, Yamamoto Y, Maehara T, Naohara T and Kawachi K: Novel tumor-ablation device for liver tumors utilizing heat energy generated under an alternating magnetic field. J Gastroenterol Hepatol 23: 1105-1111, 2008.
16. Chertok B, David AE and Yang VC: Brain tumor targeting of magnetic nanoparticles for potential drug delivery: effect of administration route and magnetic field topography. J Control Release 155: 393-399, 2011.
17. Lu ZR, Ye F and Vaidya A: Polymer platforms for drug delivery and biomedical imaging. J Control Release 122: 269-277, 2007.
18. Gan KH, Lin CN and Won SJ: Cytotoxic principles and their derivatives of Formosan Solanum plants. J Nat Prod 56: 15-21, 1993.
19. Alzérreca A and Hart G: Molluscicidal steroid glycoalkaloids possessing stereoisomeric spirosolane structures. Toxicol Lett 12: 151-155, 1982.
20. Xie X, Zhu H, Yang H, Huang W, Wu Y, Wang Y, Luo Y, Wang D and Shao G: Solamargine triggers hepatoma cell death through apoptosis. Oncol Lett 10: 168-174, 2015.
21. Kuo KW, Hsu SH, Li YP, Lin WL, Liu LF, Chang LC, Lin CC, Lin CN and Sheu HM: Anticancer activity evaluation of the solanum glycoalkaloid solamargine. Triggering apoptosis in human hepatoma cells. Biochem Pharmacol 60: 1865-1873, 2000.
22. Liang CH, Shiu LY, Chang LC, Sheu HM and Kuo KW: Solamargine upregulation of Fas, downregulation of HER2, and enhancement of cytotoxicity using epirubicin in NSCLC cells. Mol Nutr Food Res 51: 999-1005, 2007.
23. Yang X, Zhang X, Ma Y, Huang Y, Wang Y and Chen Y: Superparamagnetic graphene oxide-Fe$_3$O$_4$ nanoparticles hybrid for controlled targeted drug carriers. J Mater Chem 19: 2710-2714, 2009.
24. Liang C-C, Park AY and Guan J-L: In vitro scratch assay: A convenient and inexpensive method for analysis of cell migration in vitro. Nat Protoc 2: 329-333, 2007.
25. Livak KJ and Schmittgen TD: Analysis of relative gene expression data using real-time quantitative PCR and the 2(-Delta Delta C(T)) Method. Methods 25: 402-408, 2001.
26. van Rij CM, Frielink C, Goldenberg DM, Sharkey RM, Lütje S, McBride WJ, Oyen WJ and Boerman OC: Pretargeted radioimmunotherapy of prostate cancer with an anti-TROP-2xanti-HSG bispecific antibody and a (177)Lu-labeled peptide. Cancer Biother Radiopharm 29: 323-329, 2014.
27. Liao MY, Kuo MY, Lu TY, Wang YP and Wu HC: Generation of an anti-EpCAM antibody and epigenetic regulation of EpCAM in colorectal cancer. Int J Oncol 46: 1788-1800, 2015.
28. Wanebo HJ, Glicksman AS, Vezeridis MP, Clark J, Tibbetts L, Koness RJ and Levy A: Preoperative chemotherapy, radiotherapy, and surgical resection of locally advanced pancreatic cancer. Arch Surg 135: 81-87, discussion 88, 2000.
29. Kalra AV and Campbell RB: Development of 5-FU and doxorubicin-loaded cationic liposomes against human pancreatic cancer: Implications for tumor vascular targeting. Pharm Res 23: 2809-2817, 2006.
30. Zhang L, Chang CJ, Bacus SS and Hung M-C: Suppressed transformation and induced differentiation of HER-2/neu-overexpressing breast cancer cells by emodin. Cancer Res 55: 3890-3896, 1995.
31. Shiu LY, Chang LC, Liang CH, Huang YS, Sheu HM and Kuo KW: Solamargine induces apoptosis and sensitizes breast cancer cells to cisplatin. Food Chem Toxicol 45: 2155-2164, 2007.
32. Liu LF, Liang CH, Shiu LY, Lin WL, Lin CC and Kuo KW: Action of solamargine on human lung cancer cells - enhancement of the susceptibility of cancer cells to TNFs. FEBS Lett 577: 67-74, 2004.
33. Fisher DE: Apoptosis in cancer therapy: Crossing the threshold. Cell 78: 539-542, 1994.
34. Ho A and Dowdy SF: Regulation of G$_1$ cell-cycle progression by oncogenes and tumor suppressor genes. Curr Opin Genet Dev 12: 47-52, 2002.
35. Schimmer AD, Welsh K, Pinilla C, Wang Z, Krajewska M, Bonneau MJ, Pedersen IM, Kitada S, Scott FL, Bailly-Maitre B, *et al*: Small-molecule antagonists of apoptosis suppressor XIAP exhibit broad antitumor activity. Cancer Cell 5: 25-35, 2004.
36. Li F, Ambrosini G, Chu EY, Plescia J, Tognin S, Marchisio PC and Altieri DC: Control of apoptosis and mitotic spindle checkpoint by survivin. Nature 396: 580-584, 1998.
37. Coates PJ, Hales SA and Hall PA: The association between cell proliferation and apoptosis: Studies using the cell cycle-associated proteins Ki67 and DNA polymerase alpha. J Pathol 178: 71-77, 1996.
38. Ouhtit A, Gaur RL, Abdraboh M, Ireland SK, Rao PN, Raj SG, Al-Riyami H, Shanmuganathan S, Gupta I, Murthy SN, *et al*: Simultaneous inhibition of cell-cycle, proliferation, survival, metastatic pathways and induction of apoptosis in breast cancer cells by a phytochemical super-cocktail: Genes that underpin its mode of action. J Cancer 4: 703-715, 2013.
39. Shirali S, Aghaei M, Shabani M, Fathi M, Sohrabi M and Moeinifard M: Adenosine induces cell cycle arrest and apoptosis via cyclinD1/Cdk4 and Bcl-2/Bax pathways in human ovarian cancer cell line OVCAR-3. Tumour Biol 34: 1085-1095, 2013.
40. Pàez-Ribes M, Allen E, Hudock J, Takeda T, Okuyama H, Viñals F, Inoue M, Bergers G, Hanahan D and Casanovas O: Antiangiogenic therapy elicits malignant progression of tumors to increased local invasion and distant metastasis. Cancer Cell 15: 220-231, 2009.
41. Fang W, Li H, Kong L, Niu G, Gao Q, Zhou K, Zheng J and Wu B: Role of matrix metalloproteinases (MMPs) in tumor invasion and metastasis: Serial studies on MMPs and TIMPs. Beijing Da Xue Xue Bao Yi Xue Ban 35: 441-443, 2003 (In Chinese).
42. Chetty C, Bhoopathi P, Joseph P, Chittivelu S, Rao JS and Lakka S: Adenovirus-mediated small interfering RNA against matrix metalloproteinase-2 suppresses tumor growth and lung metastasis in mice. Mol Cancer Ther 5: 2289-2299, 2006.
43. Luca M, Huang S, Gershenwald JE, Singh RK, Reich R and Bar-Eli M: Expression of interleukin-8 by human melanoma cells up-regulates MMP-2 activity and increases tumor growth and metastasis. Am J Pathol 151: 1105-1113, 1997.
44. Hay N: The Akt-mTOR tango and its relevance to cancer. Cancer Cell 8: 179-183, 2005.
45. Altomare DA, Wang HQ, Skele KL, De Rienzo A, Klein-Szanto AJ, Godwin AK and Testa JR: AKT and mTOR phosphorylation is frequently detected in ovarian cancer and can be targeted to disrupt ovarian tumor cell growth. Oncogene 23: 5853-5857, 2004.
46. Uesugi A, Kozaki K, Tsuruta T, Furuta M, Morita K, Imoto I, Omura K and Inazawa J: The tumor suppressive microRNA miR-218 targets the mTOR component Rictor and inhibits AKT phosphorylation in oral cancer. Cancer Res 71: 5765-5778, 2011.
47. Kitano H, Chung JY, Ylaya K, Conway C, Takikita M, Fukuoka J, Doki Y, Hanaoka J and Hewitt SM: Profiling of phospho-AKT, phospho-mTOR, phospho-MAPK and EGFR in non-small cell lung cancer. J Histochem Cytochem 62: 335-346, 2014.
48. Morgensztern D and McLeod HL: PI3K/Akt/mTOR pathway as a target for cancer therapy. Anticancer Drugs 16: 797-803, 2005.
49. Takahashi M and Kohda H: Diagnostic utility of magnetic resonance imaging in malignant melanoma. J Am Acad Dermatol 27: 51-54, 1992.